

EPJ D

Atomic, Molecular,
Optical and Plasma Physics

EPJ.org

your physics journal

Eur. Phys. J. D (2014) 68: 224

DOI: [10.1140/epjd/e2014-50052-4](https://doi.org/10.1140/epjd/e2014-50052-4)

Influence of water conductivity on particular electro spray modes with dc corona discharge – optical visualization approach

Branislav Pongrác, Hyun-Ha Kim, Nobuaki Negishi and Zdenko Machala

 edp sciences



 Springer

Influence of water conductivity on particular electro spray modes with dc corona discharge – optical visualization approach

Branislav Pongráč^{1,2,a}, Hyun-Ha Kim², Nobuaki Negishi², and Zdenko Machala¹

¹ Division of Environmental Physics, Faculty of Mathematics, Physics and Informatics, Comenius University, 842 48 Bratislava, Slovakia

² Institute for Environmental Management Technology, AIST, Tsukuba, Japan

Received 17 January 2014 / Received in final form 14 May 2014

Published online 12 August 2014 – © EDP Sciences, Società Italiana di Fisica, Springer-Verlag 2014

Abstract. The effect of water conductivity on electro spraying of water was studied in combination with positive DC corona discharge generated in air. We used a point-to-plane geometry of electrodes with a hollow syringe needle anode opposite to the metal mesh cathode. We employed total average current measurements and high-speed camera fast time-resolved imaging. We visualized the formation of a water jet (filament) and investigated corona discharge behavior for various water conductivities. Depending on the conductivity, various jet properties were observed: pointy, prolonged, and fast spreading water filaments for lower conductivity; in contrast to rounder, broader, and shorter quickly disintegrating filaments for higher conductivity. The large acceleration values (4060 m/s² and 520 m/s² for 2 μS/cm and 400 μS/cm, respectively) indicate that the process is mainly governed by the electrostatic force. In addition, with increasing conductivity, the breakdown voltage for corona-to-spark transition was decreasing.

1 Introduction

Electrospray of liquids (also referred to as electrohydrodynamic atomization, EHDA) has been the subject of extensive research during the last decades [1–6]. The electro spraying effect can be generally explained as follows. When a liquid (in our case water) flows through the nozzle with no applied voltage, droplets with regular rounded shapes are formed from the end of the nozzle. The droplet size is given by the balance of capillary and gravitational force. When a voltage is applied on the nozzle, electric forces take effect. With increasing voltage, the effective surface tension of the liquid decreases due to the presence of the electric field separating positive and negative charges inside the liquid. The charges of the polarity of the high-voltage electrode move towards the droplet surface and induce a surface charge density, causing an increase of the electrostatic pressure against the capillarity pressure. When the voltage reaches a critical value, the shape of the droplet changes into conical, which is referred to as Taylor cone [2]. Subsequently, a jet emerges from the tip of the Taylor cone and breaks into droplets by various instabilities. These charged droplets are then accelerated by the electric field. Coulomb repulsion takes effect between them and the electro spraying effect occurs.

The process mentioned above is also known as a cone-jet mode of electro spraying which is relatively stable with a relative monodispersity (equal-size) of droplets [7,8].

The size of the primary droplets is generally determined by the jet radius. However, the primary droplets

may further explode if the charge they carry exceeds the Rayleigh limit for instability, which is given by [9]:

$$q_R = 8\pi\sqrt{\varepsilon_0\gamma r^3}, \quad (1)$$

where q_R is the charge on the droplet, γ the surface tension of the liquid, and r is the radius of the droplet.

Observing the cone-jet mode in liquids with higher surface tension (e.g. water) in atmospheric air can be difficult since the normal electric field E_n required to form this mode increases with the surface tension γ [10]:

$$E_n \sim \sqrt{\left(\frac{\gamma}{\varepsilon_0 R_j}\right)}, \quad (2)$$

where R_j is the jet radius, which depends on both the flow rate and the electrical conductivity of the liquid.

Therefore, the voltage required for the cone-jet mode of electro sprayed water can be higher than the electric breakdown threshold of the surrounding gas, and a disruptive electric discharge could ensue [7,10,11]. However, depending on various parameters, several other modes of electro spraying can be generated (e.g. dripping, spindle, simple jet)¹ [12,13]. It is possible to generate these modes with water, too.

¹ Dripping, spindle, or simple jet modes may not be considered “*electrospray per se*” by some authors, since there is not a large disparity of scales between the jet and the liquid meniscus, especially due to larger liquid flow rates. Nevertheless, many recent works include these modes among electro spray modes, thus we comply with this trend.

^a e-mail: branislav.pongrac@gmail.com

In the last few decades, there have been a great numbers of publications on scientific studies and practical applications of electrospray in various areas, such as ionization sources in mass spectrometry, production of micro- and nanoparticles, fuel atomization, surface coating, electro-spinning and many others [14].

One of the potential uses of water electrospray, especially large flow rate modes, is a decontamination of water from organic and microbial pollutants. The presence of an electrical discharge generating non-thermal plasma in the spraying zone allows for very efficient mass transfer of plasma-generated species into water. This method was tested in previous works of our group [15–18]. Briefly, the electrospraying of contaminated water through the corona active zone contributed to the improved efficiency of bio-decontamination in terms of treatment time and relatively low energy costs. Also a significant enhancement of bactericidal plasma effects combined by electrospraying of water was investigated on surfaces with biofilm (e.g. plastic surfaces, teeth).

When water is used as a liquid for electrospray, the electrical discharge is usually present because water has a relatively high surface tension. And since the electric field and so the voltage required to form the spray increase with the surface tension, the electrospray can occur after the corona onset voltage.

In this paper, the effect of water conductivity on the particular electrospray modes in combination with positive DC corona discharge is investigated. Generally, the conductivity of the liquid is a very important parameter affecting the surface charge at the liquid surface and has a significant effect on electrospray behavior in the cone-jet mode [19]. It is well known from many theoretical and experimental studies; e.g. [3,7,20] among others, that for a liquid of a given conductivity, the cone-jet mode appears only within a limited range of flow rates. As the conductivity increases, the boundaries of this range move towards lower flow rate, which is accompanied by a reduction of the jet diameter.

However, for some other modes of electrospraying; especially with the presence of the discharge, the reduction of the jet diameter with increasing liquid conductivity may not be always valid. Such phenomena have been partially investigated or observed by previous authors [4,5,21,22]. Nowadays, their explanations can be verified or observed more precisely by modern visualization techniques. For this purpose we used high-speed camera visualization. The advantage of this method is a time-resolved visualization of fast phenomena that are normally very hard to detect by naked eye or standard digital camera with low frame rate. Our main objective was to investigate and explain the spray behavior and especially the water filament (water jet) formation in dependence on the water conductivity. The discharge generation and its behavior during this process of electrospraying were also investigated. To our best knowledge, the influence of the conductivity of electrosprayed liquid on the discharge itself has not been investigated in detail and there is still lot of unknown in this area.

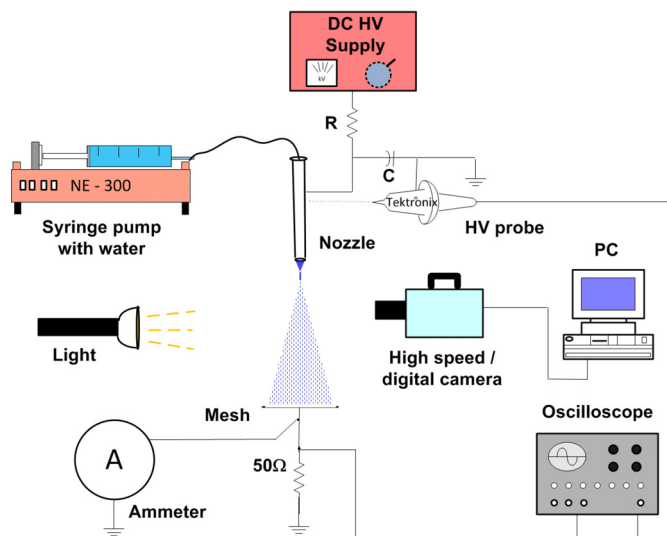


Fig. 1. Experimental set-up for investigations of electrospray of water, with a high-voltage hollow needle (nozzle) electrode enabling water flow into the inter-electrode space.

2 Experimental set-up

The experimental set-up used for the study of the influence of the water conductivity on the electrospray with DC corona discharge is shown in Figure 1. The electrodes were in point-to-plane geometry with a blunt hollow needle anode (nozzle) opposite to the mesh cathode, both stainless steel. The inter-electrode gap distances were 1, 2, or 5 cm. The nozzles were of 0.7 mm outer, 0.5 mm inner diameter for water filament observation, and 0.8 mm outer, 0.6 mm inner diameter for the discharge observation. The water was continuously supplied to the nozzle by a syringe pump NE-300 with an adjustable flow rate. In most of our experiments we used 0.4, 0.5, and 4 ml/min. As liquid media we used either deionized water with lower conductivity or NaCl water solution with higher conductivities. The conductivity of water was varied from $2 \mu\text{S}/\text{cm}$ (semi-conducting) up to $29\,000 \mu\text{S}/\text{cm}$ (highly conducting) and it was measured using a conductivity meter (Mettler Toledo).

A positive DC discharge was generated by a DC power supply applied through a ballast resistor R ($20 \text{ M}\Omega$). The discharge voltage was measured by a high-voltage probe Tektronix P6015A. The total average current was measured by an ammeter and the current and voltage signals were processed by a digitizing oscilloscope Tektronix TDS 2024 (200 MHz).

Optical visualization was used as the main method for the investigation of these fast phenomena. We used a high-speed camera Photron FASTCAM SA KH5 for the observation of dynamic processes in electrospraying. The following settings were kept for all measurements: the shutter exposure time $1 \mu\text{s}$, resolution of 384×1024 pixels with $10\,000 \text{ fps}$ (frames per second). We used a zoom lens VR Micro-Nikkor (105 mm , $f/2.8\text{G}$) attached to the high-speed camera, as a focusing and zoom optical system.

A digital camera Casio EX-F1 was used for the recording the discharge images.

3 Results and discussion

3.1 Influence of the liquid conductivity on the electrospray

Conductivity of the liquid is a significant parameter that influences the electrospray and its behavior. It is well-known that the conductivity is a degree of concentration of free ions with specific charge in the liquid. Usually, when the concentration of ions is very small and so the conductivity is very low ($<10^{-7} \mu\text{S}/\text{cm}$), no droplet deformation can be observed in electric fields. It is because the surface charge is too small and thus no appreciable deforming force can build up at the liquid-air interface [3]. With the increasing conductivity, the charge on the surface increases and the droplet deformation occurs. In this case, the droplet can be deformed into the conical shape. When the liquid has a relatively low conductivity, an electric potential difference between the base (end) of the capillary (nozzle) and the end of the liquid filament can exist. This potential drop ensures that the liquid-air interface is subjected to a tangential electric field E_t and a tangential electrical shear stress in the direction of the flow [4,5,22,23], as can be seen in the following formula:

$$E_t \sim \frac{1}{\sigma} \left(\frac{i}{\pi R_j^2} \right), \quad (3)$$

where σ is the conductivity of the liquid, i is the current in the jet and R_j is the jet radius. From this formula one can calculate the tangential electric field on the liquid surface if the total current flowing through the cone-jet is known. However, in our case the electrospraying was merged with the presence of an electric discharge; thus the total current is the superposition of the dominant discharge current and the current of ions movement in the filament. In this situation it is hard to distinguish between these two components. For high conductivity liquids, such as regular tap water ($\sim 400 \mu\text{S}/\text{cm}$), the liquid surface can be almost equipotential. Although the surface is charged, it is not subjected to a significant tangential electric field and a tangential electric shear stress. Instead, it is subjected to a normal electric field and a normal stress which tends to destabilize the propagating water filament or a jet [5]. The liquid should not be equipotential when its conductivity is below the range of $10 \mu\text{S}/\text{cm}$ [24].

In dependence on the water conductivity we observed different filament shapes and behaviors as can be seen in the following figures.

In the first set of measurements (Figs. 2 and 3) with the parameters (gap 5 cm, water flow rate 0.4 ml/min, voltage +11 kV), no permanent jet occurred. The jet was just periodically forming from the cone tip by its prolongation and was subsequently tearing off from the water meniscus as a thin liquid filament. This is described in the literature as a spindle mode of electrospraying [12,13].

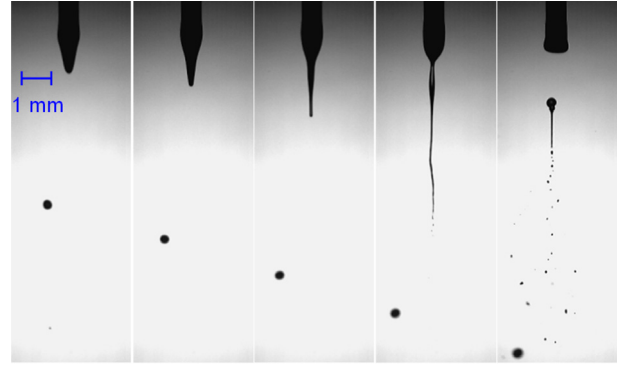


Fig. 2. High-speed camera sequence of the spindle mode electrospray with low conductivity $2 \mu\text{S}/\text{cm}$ water (10 000 fps, $1 \mu\text{s}$ gate time, time interval $700 \mu\text{s}$, flow rate 0.4 ml/min, voltage +11 kV, 5 cm gap).

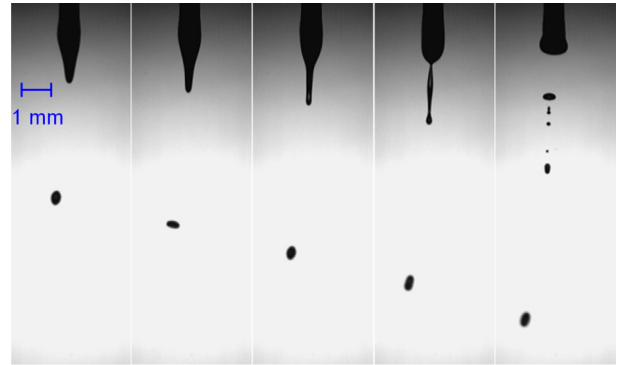


Fig. 3. High-speed camera sequence of the spindle mode electrospray with high conductivity $400 \mu\text{S}/\text{cm}$ water (10 000 fps, $1 \mu\text{s}$ gate time, time interval $700 \mu\text{s}$, flow rate 0.4 ml/min, voltage +11 kV, 5 cm gap).

After this detachment, the filament disintegrated into small droplets under the action of surface tension forces and the water meniscus shrank back to the nozzle. In Figure 2, deionized water with conductivity $2 \mu\text{S}/\text{cm}$ was used, which is much lower than $400 \mu\text{S}/\text{cm}$ shown in Figure 3. Both image sequences were taken starting right after the cone creation at the end of the nozzle until the detachment of the water filament from the main water meniscus and its following disintegration. In both figures, the time step between single images was $700 \mu\text{s}$. It can be seen that with $2 \mu\text{S}/\text{cm}$ conductivity (Fig. 2), the water filament is of significantly different shape, more prolonged and thinner at the filament head, in comparison with $400 \mu\text{S}/\text{cm}$ (Fig. 3), where the filament is shorter with the rounded thicker filament head. Because the size of droplets is directly proportional to the diameter of the filament, low conductivity water ($2 \mu\text{S}/\text{cm}$) produced smaller droplets than the high conductivity water ($400 \mu\text{S}/\text{cm}$).

With a closer look at Figures 2 and 3, the parts of the filaments under the nozzle (~ 2 mm from the nozzle) are similar for both conductivities; however the bottom parts (i.e. the filament heads) are significantly different. This different behavior can be due to the discharge presence in

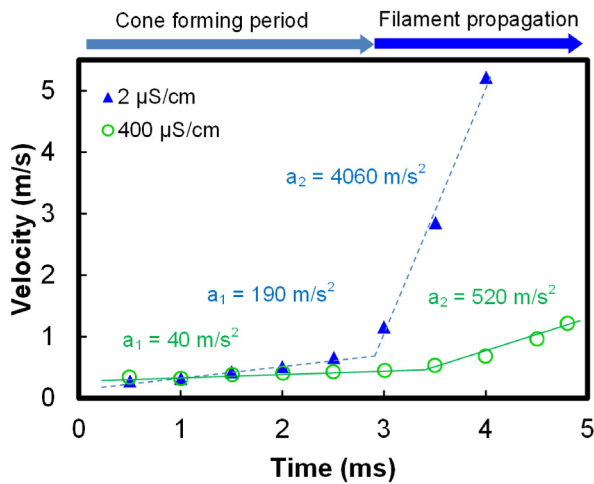


Fig. 4. Comparison of water filament velocities during the cone formation and filament propagation for 2 different conductivities.

the proximity of water surface. This is discussed in more details in Section 3.3.

With a close examination of previous figures we can notice that the velocity of water filament head propagation strongly depends on the conductivity. Because both image sequences were recorded by the high-speed camera with the same time interval, we were able to calculate the velocity of water filament propagation, as shown in Figure 4. The velocity was calculated for a number of points as a difference of water filament lengths over exact times, until the water filament detached from the nozzle. The velocity-time curves are divided into two main areas: the slower area with lower propagation velocities (in Fig. 4 from 0 to 3 ms, marked as Cone forming period), where the cone is still forming and starts to transform into filament, and the faster area with higher propagation velocities (in Fig. 4 from 3 ms higher, marked as filament propagation), where the filament is propagating towards the ground electrode until its disintegration. One can see that for the lower conductivity (blue triangles), the velocity-time curve is more exponential in comparison with higher conductivity (green circles). It means that the acceleration and probably the acting force are higher too, as can be seen from the calculated acceleration values in Figure 4.

This is very likely caused by the effect of different tangential electric fields and resultant tangential electric forces mentioned above. In addition, the rates of acceleration in the filament front during the filament propagation period were 4060 m/s^2 and 520 m/s^2 for $2 \text{ } \mu\text{S/cm}$ and $400 \text{ } \mu\text{S/cm}$, respectively, which are greatly far above the gravitational acceleration (9.8 m/s^2). This clearly indicates that the process is mainly governed by the electrostatic force and the gravitational force can be neglected.

The similar effect of different filament behavior for different conductivities can be also seen in the case (Figs. 5 and 6) with higher liquid flow rate of 4 ml/min (gap 5 cm , voltage $+14 \text{ kV}$). In this case, the jet was permanent in terms that no water filament was periodically detached

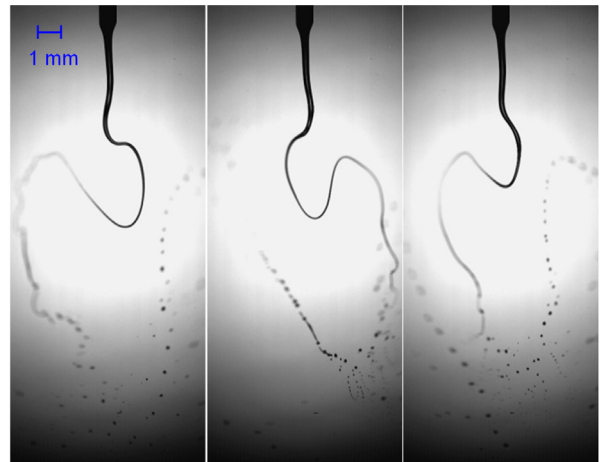


Fig. 5. High-speed camera sequence of the oscillating simple jet electro spray with low conductivity $2 \text{ } \mu\text{S/cm}$ water (10000 fps, $1 \text{ } \mu\text{s}$ gate time, time interval $800 \text{ } \mu\text{s}$, flow rate 4 ml/min , voltage $+14 \text{ kV}$, 5 cm gap).

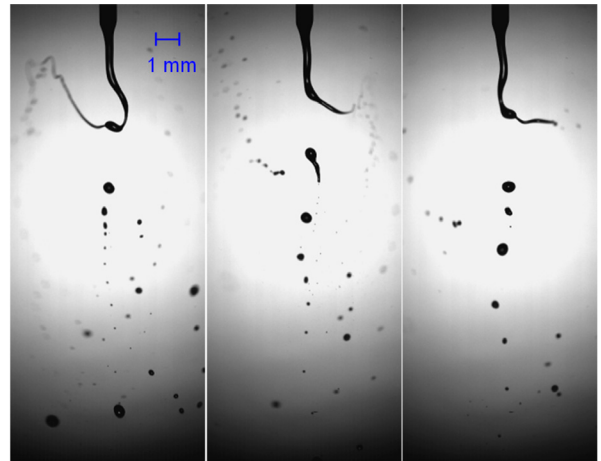


Fig. 6. High-speed camera sequence of the oscillating simple jet electro spray with high conductivity $400 \text{ } \mu\text{S/cm}$ water (10000 fps, $1 \text{ } \mu\text{s}$ gate time, time interval $800 \text{ } \mu\text{s}$, flow rate 4 ml/min , voltage $+14 \text{ kV}$, 5 cm gap).

from the main meniscus but it was permanently connected with the high-voltage electrode [12]. In the absence of an electric field, the liquid would also form a permanent jet if the kinetic energy of the liquid at the outlet of the capillary was greater than the surface energy required to create the surface of the jet [25]. In our case, the application of high voltage has a stabilizing effect on the already established jet that gradually prolongs.

Although the jet was permanent, it started to oscillate in horizontal direction probably due to the repulsive action of higher surface charge on the jet due to the higher currents caused by the high imposed flow rate (similar to kink instabilities in the cone-jet mode disintegration) [6,7,26]. According to the literature it corresponds to an oscillating simple jet mode of electro spraying [12,13], and these whipping motions can be also caused by the deflection of the jet off the capillary axis due to the field generated by formerly emitted charged droplets or ions [13], and by additional

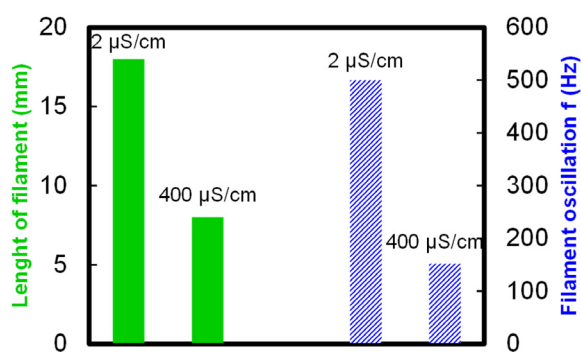


Fig. 7. Comparison of water filament lengths (left filled section) and filament oscillation frequencies (right lined section) for 2 different conductivities (oscillating simple jet mode, flow rate 4 ml/min, 5 cm gap).

mechanical forces due to the fast filament propagation velocity and resultant drag force of surrounding air [27]. The initial lateral oscillations with low amplitude can be seen already a few millimeters under the nozzle. The increase of lateral whipping amplitude with the jet diameter reduction (mass of the filament fragment is lower) can be explained by the law of momentum conservation.

The simple jet and cone-jet exhibit similar structures. Both consist of a single jet drawn from the meniscus by the electrical forces. The simple jet differs from the cone-jet in the sharpness of the conical meniscus (there is no significant transition between the cone and the jet in the simple jet mode).

The effect of conductivity on the jet shape is still visible, as can be seen in Figures 5 and 6 for the two tested conductivities: 2 and 400 μS/cm, respectively. At lower conductivity, the oscillating jet disintegrated at greater length than at higher conductivity and had a thin head. For higher conductivity, the head of the jet was again thicker and more rounded.

The length of the jet was measured from the base (end) of the capillary to the beginning of the jet disintegration. These results are summarized in the left section of Figure 7. We can see that for the lower conductivity, the jet is almost 3 times longer than for the higher conductivity. Interesting phenomena can be also seen in the right section of Figure 7. Since the filament performs relatively regular lateral oscillation movements, we calculated the time period and so the frequency of these vigorous movements.

We measured the time period of one oscillation from the high-speed camera sequence and subsequently converted it to the frequency. At the lower conductivity, the frequency was almost 4 times higher compared with the higher conductivity due to the faster water flow in the narrower filament.

These experimental results are in a good qualitative agreement with the theory and previous published results mentioned at the beginning of this section. Generally, low water conductivity results in elongation of the water filament due to the presence of tangential electric field and tangential electric shear stress. Higher conductivity results in shorter water filaments due to the negligible effect of tangential electric field.

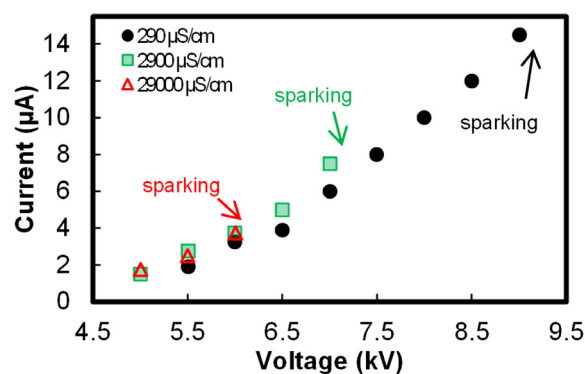


Fig. 8. Current-voltage characteristics of the electro spray with corona discharge ($d = 1$ cm, $Q = 0.4$ ml/min). Different breakdown voltages for corona-to-spark transition are due to different conductivity effect.

3.2 Influence of the liquid conductivity on the discharge properties

In this section, another effect of the conductivity will be demonstrated from the perspective of corona discharge generation during the electro spray. According to the literature, various conductivities of the sprayed water can affect the space charge distribution in the discharge zone and intensities of the electric field at the liquid surface [28]. Also, in more conductive liquids, the discharge should more likely take place from the liquid surface, which has almost the same potential as the electrode. In more insulating liquids, the discharge occurs more likely at the metal tip [4]. These effects can cause some differences in the discharge behavior for various conductivities of the sprayed water.

We detected the corona discharge starting from about 4.5 kV in 1 cm gaps.

Interesting results are demonstrated in Figures 8 and 9 for 1 and 2 cm gap distances, respectively. With the increasing voltage, the total average current values were measured for 3 different water conductivities: 290; 2900; and 29000 μS/cm. Measurement was carried out from the lowest current values until the sparking occurred. Subsequently, a V - I characteristics were plotted. As can be seen in Figure 8 for 1 cm gap, when the conductivity is increasing, the breakdown voltage for corona-to-spark transition is decreasing. The same behavior can be seen in Figure 9 for 2 cm gap, but with different current values.

Considering the spray behavior shown in Figures 2 and 3, this phenomenon can be explained as follows: since the highly conductive liquid acts as a relatively good conductor, the electric field should be stronger on the highly conductive water meniscus. The discharge is thus permitted to occur at the liquid surface and the discharge activity on the water filament tip is then enhanced as the filament proceeds toward the ground electrode and reduces the effective gap distance. For better understanding, this process is similar to the reduction of gap distance by shifting the position of the HV needle electrode towards the ground electrode. During this process, the filamentary

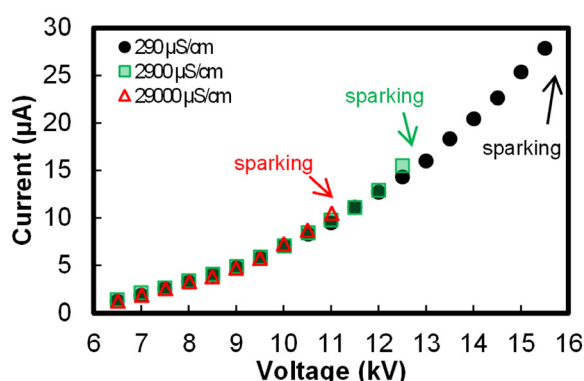


Fig. 9. Current-voltage characteristics of the electro spray with corona discharge ($d = 2$ cm, $Q = 0.4$ ml/min). Different breakdown voltages for corona-to-spark transition are due to different conductivity effect.

streamer discharge can occur from the tip through the entire gap space which can eventually facilitate the spark generation at a relatively low voltage. On the other hand, for poorly conductive liquids, the liquid acts more as an insulator and the electrical resistance of the growing water filament suppresses the corona activity on its surface. Therefore, the corona space charge is prevented from accumulating on the propagated filament surface and so the discharge is forced to occur on the metal electrode. Subsequently, the spark does not occur until the higher voltage [22,29].

Additionally, the above mentioned breakdown voltage reduction causes another effect. During this observation we used a slightly different HV electrode with sharper edges promoting the discharge generation from the electrodes edges. We observed that due to the previously mentioned decreasing breakdown voltage with increasing conductivity, the evolution of an intense streamer corona was prevented with the increasing water conductivity, as can be seen in Figure 10.

It means that for the high liquid conductivities (in our case more than $1000 \mu\text{S/cm}$), the frequency of streamer generation cannot be reached too high because the streamer regime transits to spark at relatively low voltage when the frequency of streamers is still too low. This is caused by the above mentioned effect of enhanced corona discharge activity on the tip of water filament which eventually facilitates the spark from this tip at lower voltages [22]. On the other hand, the streamer-to-spark transition at lower voltage is prevented for low liquid conductivities (in our case less than $100 \mu\text{S/cm}$). Since the liquid acts more as an insulator and tends to suppress the corona activity on the tip of the water filament and prevents the sparking in the low voltage; with the increasing voltage the discharge is forced to occur on the metal electrode [22]. It is then possible to reach higher voltages without any sparks from the water filament tip and the discharge tends to occur more likely from the sharp edges of the HV electrode. Thus, with the increasing voltage of low conductivity liquid, the frequency of the streamers can reach relatively high value before the spark break-

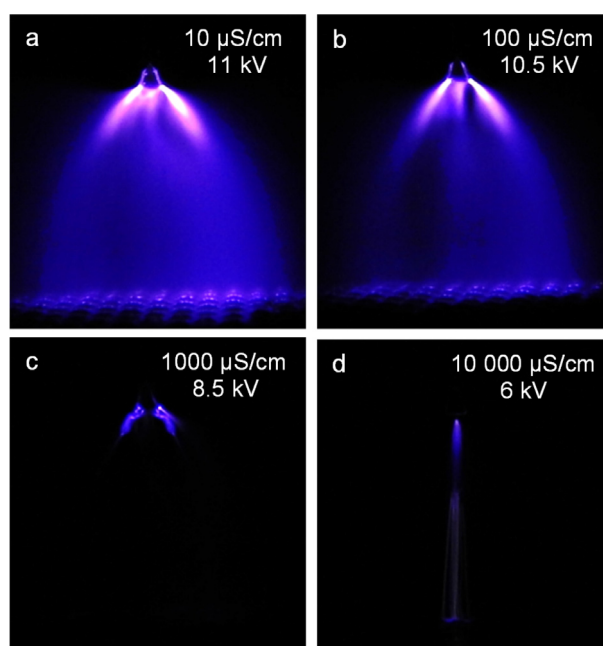


Fig. 10. Conductivity effect on the corona discharge with electro spray in maximum pre-breakdown voltages (the streamer current frequency of image (a) is 5.6 kHz, (b) is 4.4 kHz, (c) is 0.32 kHz, and (d) is 0.65 kHz), $d = 1$ cm, $Q = 0.5$ ml/min.

down, since the streamer frequency commonly increases with the applied voltage.

This result is important to consider in applications of the electro spray with the discharge for water decontamination mentioned in the introduction.

3.3 Influence of the corona discharge on the water filament

Since the increasing liquid conductivity facilitates the discharge presence on the water tip, its resultant ionic space charge in the proximity of the water meniscus can significantly affect the surface electric field and the shape of the filament tip. As shown in Figure 3, the end of the water filament is not as pointy for higher conductivity as for the lower conductivity in Figure 2, but it is more rounded with smaller curvature.

This can be explained by an enhanced discharge activity near the conducting liquid filament which acts as a conductor. During the propagation of the filament along the gap, the surface electric field on the filament head becomes more reduced with the enhanced discharge activity due to the ionic space charge forming around the filament tip with corona discharge. On the meniscus surface, there is a balance between capillary and electric pressure which is vital for the meniscus to keep its pointed shape. When the electric field and so the electric pressure on the head of the filament becomes more reduced, the capillary pressure is also reduced. Therefore the filament tip becomes more spherical with a surface of smaller curvature and the resultant droplets formed from the disintegrated water filament

are not ordered as regularly as for the lower conductivity; smaller droplets are in front and bigger ones follow them, in agreement with [22]. The droplets are usually created as a pair of bigger droplets in the front and on the tail, and some smaller droplets between them (Fig. 3, right image).

For low conductivity liquids, the liquid acts more as an insulator. The electrical resistance of the growing filament suppresses the corona activity due to the voltage drop along the filament, preventing the corona space charge from accumulating around the filament, and so the surface electric field is not as reduced as for the conductive liquids. This results in a sharper tip of the water filament head with a surface of greater curvature. Therefore, smaller droplets are created in the front and bigger droplets on the tail (Fig. 2, right image), again in agreement with [22].

4 Conclusions

The methods of high-speed camera visualization combined with total average current measurements were used to investigate the effect of water conductivity on some particular modes of electro spraying in combination with positive corona discharge. This combination of plasma with water spray is a promising method for water treatment and decontamination. Our objective was to identify the behavior of the spray and the discharge for different conductivities of water.

The visible differences in the shape of water filaments (jets) and their formation were observed for various water conductivities. For low conductivity ($\sim 2 \mu\text{S}/\text{cm}$), the jet shape was more prolonged and thinner at the filament head, with higher velocity of propagation, when compared with higher conductivity ($\sim 400 \mu\text{S}/\text{cm}$). Generally, the droplets with smaller sizes were formed only for low conductivity, which is contrary to the well-established theory of cone-jet modes mentioned in many studies dealing with the electro spray. However, the cone-jet modes were not observed in this work with water with relatively high flow rates ($>0.4 \text{ ml}/\text{min}$) and with the presence of the electric discharge. The large acceleration values for both conductivities ($4060 \text{ m}/\text{s}^2$ and $520 \text{ m}/\text{s}^2$ for $2 \mu\text{S}/\text{cm}$ and $400 \mu\text{S}/\text{cm}$, respectively) indicate that the process is governed by the electrostatic force.

The discharge characteristics were also influenced by the conductivity. Especially the breakdown voltage for corona-to-spark transition decreased with the increasing conductivity. Due to this phenomenon, the evolution of an intense streamer corona discharge was inhibited for higher conductivities. The disturbing effect of the discharge on the shape of the water filament meniscus point was also visible: the water filament tip became more pointed with greater curvature for lower conductivity and more rounded with smaller curvature for higher conductivity. This affected the properties of the droplets resultant from the water filaments by their disintegration.

These results show the complex behavior of the water electro spray in combination with corona discharge and their mutual influence that should be considered in applications.

The authors thank Prof. V. Martišovič for his valuable comments during the preparation of this paper. This work was supported by the Slovak Research and Development Agency APVV-0134-12 and Slovak grant agency VEGA 1/0998/11.

References

1. J. Zeleny, Phys. Rev. **10**, 1 (1917)
2. G. Taylor, Proc. R. Soc. Lond. Ser. Math. Phys. Sci. **280**, 383 (1964)
3. D.P.H. Smith, IEEE Trans. Ind. Appl. **IA-22**, 527 (1986)
4. I. Hayati, A.I. Bailey, T.F. Tadros, J. Colloid Interface Sci. **117**, 205 (1987)
5. I. Hayati, A. Bailey, T.F. Tadros, J. Colloid Interface Sci. **117**, 222 (1987)
6. M. Cloupeau, B. Prunet-Foch, J. Electrostat. **25**, 165 (1990)
7. M. Cloupeau, B. Prunet-Foch, J. Electrostat. **22**, 135 (1989)
8. D.-R. Chen, D.Y.H. Pui, S.L. Kaufman, J. Aerosol Sci. **26**, 963 (1995)
9. D.C. Tafliin, T.L. Ward, E.J. Davis, Langmuir **5**, 376 (1989)
10. J.M. López-Herrera, A. Barrero, A. Boucard, I.G. Loscertales, M. Márquez, J. Am. Soc. Mass Spectrom. **15**, 253 (2004)
11. K. Tang, A. Gomez, J. Colloid Interface Sci. **175**, 326 (1995)
12. M. Cloupeau, B. Prunet-Foch, J. Aerosol Sci. **25**, 1021 (1994)
13. A. Jaworek, A. Krupa, J. Aerosol Sci. **30**, 873 (1999)
14. A.G. Bailey, *Electrostatic Spraying of Liquids* (Research Studies Press, John Wiley & Sons, Taunton, Somerset, England, New York, 1988)
15. Z. Machala, L. Chládková, M. Pelach, J. Phys. D: Appl. Phys. **43**, 222001 (2010)
16. Z. Machala, B. Tarabova, K. Hensel, E. Spetlikova, L. Sikurova, P. Lukes, Plasma Process. Polym. **10**, 649 (2013)
17. Z. Koval'ová, K. Tarabová, K. Hensel, Z. Machala, Eur. Phys. J. Appl. Phys. **61**, 24306 (2013)
18. Z. Koval'ová, M. Zahoran, A. Zahoranová, Z. Machala, J. Phys. D: Appl. Phys. **47**, 224014 (2014)
19. A.M. Gañán-Calvo, J. Dávila, A. Barrero, J. Aerosol Sci. **28**, 249 (1997)
20. J.F. De La Mora, A. Gomez, K. Tang, US Patent **5**, 873 (1999)
21. M. Mutoh, S. Kaieda, K. Kamimura, J. Appl. Phys. **50**, 3174 (1979)
22. S. Kuroda, T. Horiuchi, Jpn J. Appl. Phys. **23**, 1598 (1984)
23. A. Barrero, A.M. Gañán-Calvo, J. Dávila, A. Palacios, E. Gómez-González, J. Electrostat. **47**, 13 (1999)
24. J.F. De La Mora, J. Fluid Mech. **243**, 561 (1992)
25. N.R. Lindblad, J.M. Schneider, J. Sci. Instrum. **42**, 635 (1965)
26. R.P.A. Hartman, J.-P. Borra, D.J. Brunner, J.C.M. Marijnissen, B. Scarlett, J. Electrostat. **47**, 143 (1999)
27. H.-H. Kim, J.-H. Kim, A. Ogata, J. Aerosol Sci. **42**, 249 (2011)
28. J.-P. Borra, P. Ehouarn, D. Boulaud, J. Aerosol Sci. **35**, 1313 (2004)
29. J.P. Borra, Y. Tombette, P. Ehouarn, J. Aerosol Sci. **30**, 913 (1999)